Design and experimental performance of practical model predictive control (MPC) for multi-zone variable refrigerant system (VRF) for small and medium commercial buildings

Sang woo Ham[1]*, Donghun Kim[2], Lazlo Paul[3]

[1]Building Technology & Urban System Division, Lawrence Berkeley National Laboratory, Berkeley, CA, United States of America
sham@lbl.gov

[2]Building Technology & Urban System Division, Lawrence Berkeley National Laboratory, Berkeley, CA, United States of America
donghunkim@lbl.gov

[3]Building Technology & Urban System Division, Lawrence Berkeley National Laboratory, Berkeley, CA, United States of America
lpaul@lbl.gov

*Corresponding Author

ABSTRACT

With the urgent call for carbon reduction, the realization of grid-interactive efficient buildings (GEBs) that provide load flexibility (e.g., load shifting, peak demand reduction, etc.) has become a major research area. Model predictive control (MPC), which optimizes the operations of building heating, ventilation, and air-conditioning (HVAC) systems and distributed energy resources (DERs) based on grid conditions, is one of the mature and viable solutions for GEBs of small and medium commercial buildings (SMCBs), where the advanced building management system and sensor infrastructure are often not available. Despite the recent success of practical MPC solutions for SMCBs with simple HVAC systems such as rooftop units (RTUs), the design of MPC for a complex system such as a variable refrigerant (VRF) system is still costly. In this paper, we present a practical MPC solution for a multi-zone VRF system for small and medium commercial buildings. Utilizing heating operational data from a multi-zone laboratory office building, we propose a VRF model for heating operation and MPC structures based solely on the available data. The developed MPC solution was applied to the laboratory office building for a heating week with a dynamic pricing signal. The results indicate that the proposed MPC can achieve reductions of approximately 32% in peak demand and 3% in energy costs by shifting 24% of peak-time load to non-peak time hours, respectively.

1. INTRODUCTION

There is a notable push towards achieving a carbon-neutral society to tackle the pressing issue of climate change. As part of this transition, there's a growing focus on grid-interactive efficient buildings (GEBs) due to their significant impact on U.S. electricity consumption (over 70%) and CO2 emissions (about 40%) (Satchwell et al., 2021). Since a complete shift to renewable energy in the building sector would demand substantial financial investments, GEBs offer a pathway for decarbonization by providing flexibility in demand through various distributed energy resources (DERs) and by collaborating with the utility grid to offer services like load shifting and load shedding (Neukomm et al., 2019). The combination of decarbonization technology and load shifting to renewable energy production time is expected to a 91% reduction in carbon emissions in building sectors by 2050 (Langevin et al., 2023).

While traditional research on building control has typically concentrated on enhancing the energy efficiency of heating, ventilation, and air-conditioning (HVAC) systems (ASHRAE, 2021), more recent investigations have investigated into advanced control approaches geared towards enabling grid services through dynamic HVAC

operations like load shifting and peak demand reduction. These controls can coordinate the use of various resources (such as HVAC systems, solar PVs, and batteries) while considering external factors like grid conditions, weather patterns, and occupancy levels. They employ model-based optimal control methods such as model predictive control (MPC) or artificial intelligence techniques like reinforcement learning (RL). Recent studies of these advanced control strategies have demonstrated significant potential to lower energy costs (Touzani et al., 2021) and boost the utilization of renewable energy sources (Kim et al., 2022) in real-world buildings.

Those advanced control technologies are typically applied for large commercial buildings with centralized building automation systems (Li et al., 2015; De Coninck and Helsen, 2016; Blum et al., 2022). However, those advanced controls are not often found in small and medium commercial buildings (SMCBs, floor area less than 50,000 ft2), which take 50% of the floor area of whole commercial buildings (U.S. Energy Information Administration (EIA). 2018), because those buildings are typically equipped with relatively simpler HVAC systems such as ON/OFF rooftop units (RTU) or mini-split systems with thermostats that do not provide enough data variables and control capabilities required for them.

Several recent studies have developed and demonstrated low-cost and practical MPC solutions that do not require additional infrastructure retrofits other than WiFi-enabled thermostats for SMCBs with ON/OFF staged RTUs because the installation of centralized building automation systems for those SMCBs is costly and not desired. A plug-and-play style MPC was developed and applied for a gymnasium with 4 RTUs showing 8% energy reductions and 40% peak demand reductions by coordinating multiple RTU operations (Kim et al., 2015). The MPC solution was further improved by adopting an unmeasured disturbance model in its formulation, which makes the solution low-cost and practical, and it provided about 12% of energy and 18% of peak demand through RTU coordination for several months of trials (Kim et al., 2018). Kim and Braun (Kim et al., 2022b) integrated a load shifting feature into the MPC solution in a hierarchical MPC structure for ON/OFF staged packaged units in a laboratory building. The solution showed 30% of demand cost savings and 40% of on-peak demand cost savings with less than 10% of total energy cost savings. In addition, the solution has been demonstrated for K-12 school buildings with 6 RTUs, showing a 24% peak demand reduction during the summer season (Ham et al., 2023). Furthermore, the MPC solution was extended to a dual-fuel system (i.e., heat pumps and a gas furnace) in a small office building and eliminated gas usage during the two-month of winter demonstration period (Ham et al., 2024).

While this low-cost MPC solution is mainly applied for ON/OFF staged packaged units, it has not been developed for more complex systems such as VRF systems. A VRF system, similar to ductless mini-split heat pumps, delivers both heating and cooling to indoor areas using refrigerant as its energy transfer medium. This system functions through a refrigerant cycle operation (ASHRAE, 2020), efficiently serving numerous rooms via an outdoor unit (OU). By employing variable speed compressor control and multiple electronic expansion valves (EEVs), it optimizes part-load operations across various thermal zones. Moreover, VRF systems with heat recovery capabilities enable simultaneous heating and cooling, which proves particularly advantageous for buildings featuring thermal zones with diverse load characteristics.

The VRF system is increasingly favored in SMCBs and multi-family residential constructions, particularly when paired with a dedicated ventilation setup such as a dedicated outdoor air system (DOAS). This popularity arises from its superior performance in part-load operations, its ability to provide both heating and cooling in a single unit, its flexible zone-level controls, and its efficiency in structural design by saving duct space. With the recent nationwide push for electrification and the adoption of heat pumps, it is expected that VRF systems will gain further popularity in SMCBs. Consequently, there is a pressing need to conduct research aimed at enhancing the capabilities of low-cost MPC solutions tailored for VRF systems.

In this study, we introduce a practical MPC solution tailored for multi-zone VRF systems in small and medium commercial buildings. We gathered operational data from a VRF system installed within a laboratory office building containing 13 thermal zones. Then, we analyzed the relationship among control variables, heating and cooling rates, and electricity usage. Based on the analysis, we derived correlations between these factors to predict energy consumption by using typically available data. The correlations are integrated into our MPC solution by extending the MPC formulation. This developed solution was then implemented in the laboratory office building during a heating week under dynamic pricing conditions. Finally, we will briefly address the practical challenges associated with MPC implementation in occupied buildings and discuss future research directions aimed at developing a comprehensive MPC solution tailored for heat recovery mode.

2. VRF SYSTEM AND EXPERIMENT SITE

2.1 VRF System in Predictive Control

A VRF system consists primarily of two main components: an outdoor unit (OU) and indoor units (IUs), connected via refrigerant pipe loops. Each IU, designated to serve a specific thermal zone, comprises a heat exchanger and a fan. The heat exchanger is a core component, functioning either as an evaporator for cooling or as a condenser for heating, with the direction of refrigerant flow being reversed accordingly. The refrigerant flow within each IU is regulated by an electronic expansion valve (EEV), synchronizing with thermostat commands. IUs are available in various configurations tailored to suit the specifics of the building, such as ceiling-mounted cassettes or fan coil units.

For predictive control methods like MPC, understanding the correlation between the control variable (EEV), the heating and cooling rates supplied to the zone, and the electricity consumption of the OU is important. To investigate this relationship, we gathered operational data from a VRF system installed within an office building housing 13 thermal zones. These zones encompass various areas such as a reception desk, a conference room, two open-space offices, and several private offices. Notably, the VRF system in this building conducts both heating and cooling operations and boasts the capability of simultaneous heating and cooling through heat recovery operations.

2.2 Demonstration Site

Figure 1 illustrates a schematic diagram of the VRF system featuring heat recovery, showcasing only three zones for clarity. This system comprises three key components: the OU, branch controller, and IU. Each room, or thermal zone, is served by an IU controlled by a thermostat. For simultaneous heating and cooling tasks, the branch controller plays a crucial role. When different zones necessitate both heating and cooling simultaneously, the branch controller adjusts the refrigerant flows to cater to each zone's specific needs. However, an important constraint is that IUs under the same branch controller must operate in the same heating or cooling mode, a determination made by the system's internal logic based on aggregated thermostat information within the same branch. Among the numerous data points accessible from the VRF system, we highlight in red text the variables utilized for our data analysis.

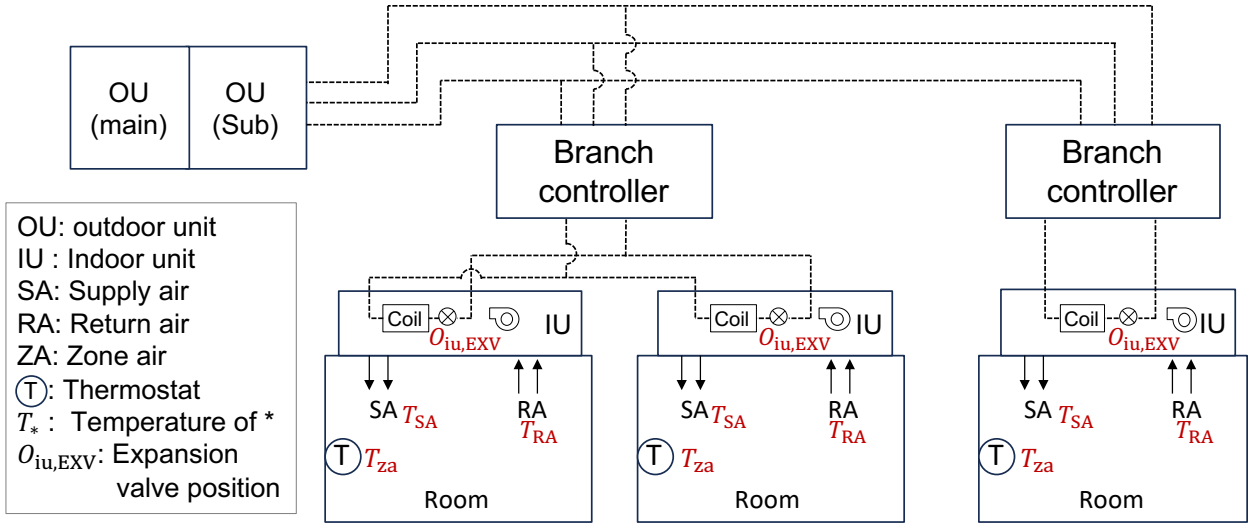

Figure 1. Schematic diagram of a VRF system with heat recovery in the demonstration site.

The thermostat sends a heating or cooling request signal to the system based on setpoints and the current zone air temperature, activating EEVs in IUs according to the internal control logic of the VRF system. While the EEV serves as a variable for directly controlling the heating and cooling rate, direct manipulation of the EEV position is typically not permitted. Instead, the internal logic of the system adjusts the EEV to meet the setpoint within a certain time interval. Therefore, we can indirectly control the EEV position by setting the corresponding setpoint for the time interval. From the data investigation, it was determined that a 30-minute interval provides sufficient sampling time for the internal logic to achieve the desired setpoint.

3. MPC FORMULATION

3.1 Heating Performance Map

We first investigated the relationship between calculated supply heating rates ($\hat{Q}_{heat}$) and scaled EEV positions for each zone in 30-minute time intervals (i.e., sampled at a 30-minute interval after moving averaging) as shown in Figure 2. Each graph shows each IU's data (i.e., thermal zone) after data processing.

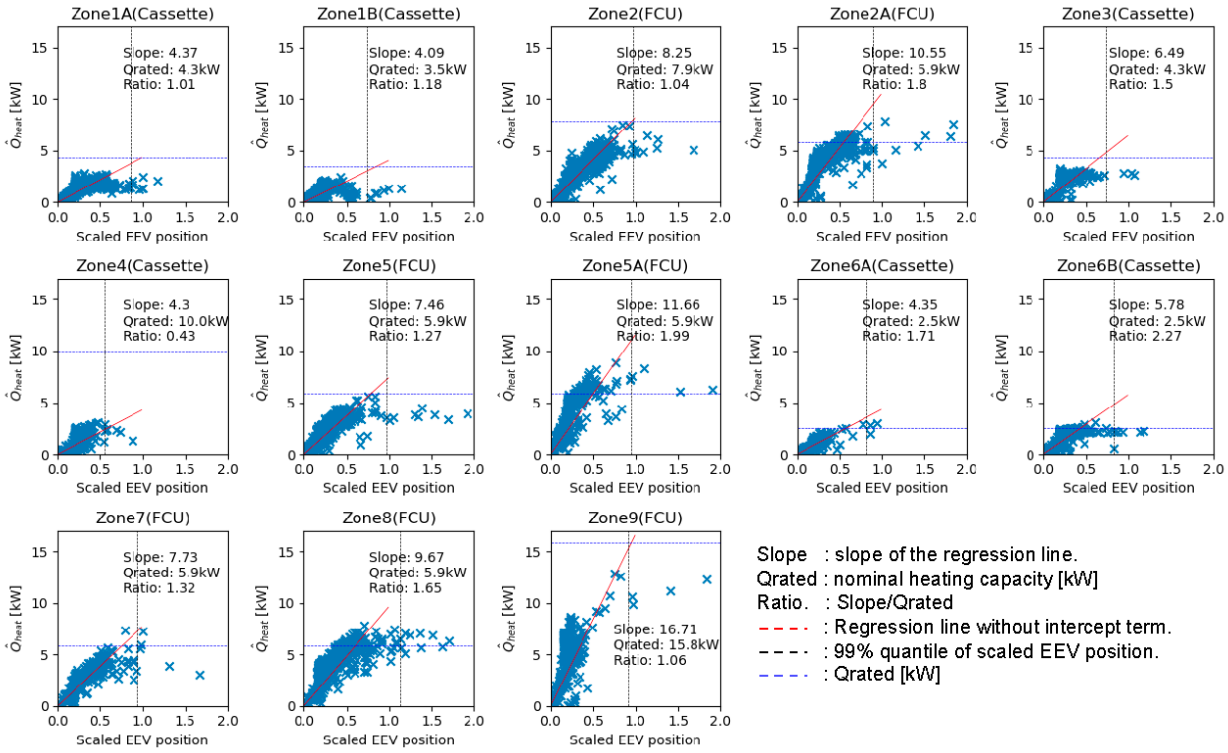

Figure 2. The relationship between supplied heating rates vs. scaled EEV positions; zone indicator and type of IU is shown at the top.

The data processing was achieved in the following steps. The maximum value of valve opening position is documented as 2500, as per the manufacturer's data, but they were typically controlled within the range of 0-1000 for most of the time after 30-minute interval sampling (based on observing the 99% quantile line, represented by the black dotted vertical line, indicating that the majority of data points fall below 1000). In some cases, it shows values higher than 1000, but the data analysis revealed it could be driven by some noisy operations such as the start-up time. Except for those special cases, the setpoint control was achieved within the range of 0-1000 for most of the time, so we set 1000 as the maximum controllable valve opening position, and the EEV position values are scaled by 1000.

The supplied heating rates were computed based on the rated airflow from the catalog data multiplied by the difference between return and supply air temperatures. From these two variables, regression lines without intercept terms (indicated by red dotted lines) were obtained. Finally, the nominal heating capacities were represented by blue dotted horizontal lines, and their values were compared with the slope of the regression lines.

The analysis revealed that the scaled EEV positions generally exhibit a linear relationship with the calculated supply heating rate, albeit with variations. These variations can be attributed to multiple factors. For instance, the cassette unit has supply air and return air grilles at the same location, resulting in numerous short circuits during heating operation. Consequently, the calculated supply heating rate from the air side is inherently noisy and may not increase regardless of the EEV position at certain points. Additionally, some FCUs serve multiple private office rooms simultaneously with one return air grille. If the private office door is closed, the supplied heating air may barely reach the return air grille, causing the FCU to draw air from nearby zones, and resulting in noisy behavior. Nonetheless,

despite these challenges, a general linear relationship was observed, and the estimated slope exhibited similar values to the nominal rated catalog values. This implies the supplied heating rates can be expressed as a function of the scaled EEV position variable in the building thermal model.

Then, the relationship between outdoor air unit power (P_{ou}) and EEV positions was investigated. In predictive control applications, predicting power consumption based on control inputs is essential. We developed 4 types of model structures based on the data analysis and physical principles, and we compared predicted values with measured values in Figure 3. The tested model cases are summarized in Table 1.

Table 1. Model cases.

Model case	Predictor (independent) variables of the linear model
Case 1	$\overline{EEV}_1^*,\ \overline{EEV}_2^*, \dots, \overline{EEV}_n^*,\ T_{oa}^*$
Case 2	$\sum_{i=1}^{n}(\dot{Q}_{heat,i}^{r}\overline{EEV}_i^*),\ T_{oa}^*$
Case 3	$T_{oa}^* \sum_{i=1}^{n}(\dot{Q}_{heat,i}^{r}\overline{EEV}_i^*)$
Case 4	$\sum_{i=1}^{n}(\dot{Q}_{heat,i}^{r}\overline{EEV}_i^*),\ T_{oa}^* \sum_{i=1}^{n}(\dot{Q}_{heat,i}^{r}\overline{EEV}_i^*)$

where $(\cdot)^*$: scaled values of a variable $(\cdot)$, n is the total number of zones, and $1,2,\dots,n$ is zone index, $\overline{EEV}_i^*$ is moving-averaged scaled EEV position of ith zone for the sampling time, T_{oa}^* is scaled outdoor air temperature ($T_{oa}/T_{oa,max}$), $T_{oa,max}$ is set to 30ºC, $\dot{Q}_{heat,i}^{r}$ is a nominal heating capacity of the IU in ith zone from the catalog data.

In all four cases, the outdoor air term is included to accommodate the performance variation of the outdoor air temperature. Case 1 includes all the individual EEV's positions as predictor variables to account for the performance variations of different EEVs. In Case 2, all the EEV positions are summed up after multiplying by the nominal heating capacity. In Case 3, the outdoor air term is directly multiplied by the summation of the nominal rated heating and EEV position value. Case 4 is a mixture of Case 2 and Case 3.

As depicted in Figure 3, Cases 1, 2, and 4 demonstrated good performance, whereas Case 3 did not. This indicates that the impact of the amount of EEV positions on power consumption is less correlated with the performance variation due to outdoor air temperature. Additionally, Cases 2 and 4 exhibited similar performance, suggesting that the inclusion of Case 3's term is not critically important in this model structure. Ultimately, Case 1 showed the best performance as it explains the variations of individual EEV's contribution to the total power. However, Case 1 requires rich operational data of all EEVs to accurately estimate all the parameters. Considering that the performance improvement by having Case 1 is not superior to Case 2, we decided to use the Case 2 model structure, as it could be more robust even when some EEVs' operational data is limited by using the nominal capacities.

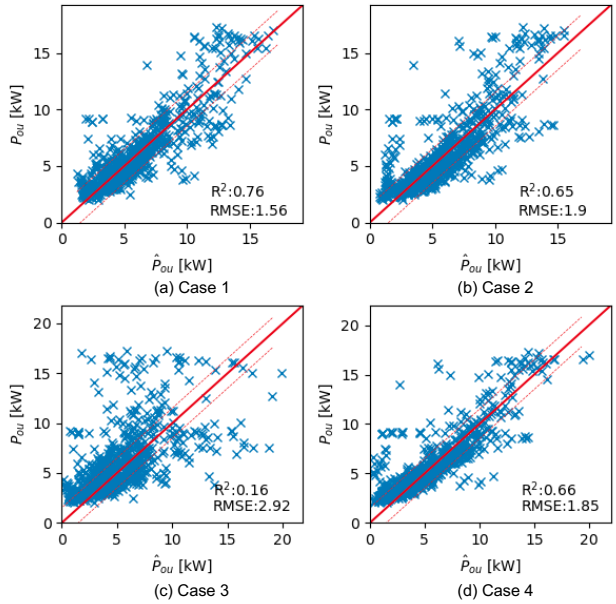

Figure 3. Predicted ($\hat{P}_{ou}$) vs. measured (P_{ou}) power of OU for different model structures.

3.2 MPC Formulation

The MPC (Kim et al., 2022a) generates the desired setpoint profile aiming to minimize energy costs through load shifting, considering future weather and utility price signals for a long-term time horizon (e.g., one day). Figure 4 illustrates the concept behind this algorithm. The MPC preheats some zones to minimize heating operations during periods of high electricity prices (peak price time). It also prevents the simultaneous operation of different units to reduce maximum demand, thus mitigating increases in electricity bills.

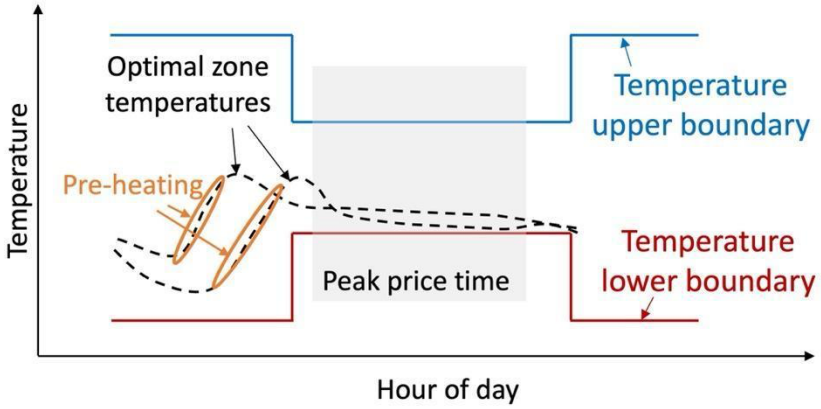

Figure 4. Conceptual diagram of the MPC for load shifting.

From the previous analysis, the Case 2 model is chosen for the VRF power prediction. The model can be expressed as Eq. (1),

$$\hat{P}_{\mathrm{ou}}(j) = \beta_{\mathrm{EEV}} \sum_{i=1}^{n} \dot{Q}^{\mathrm{r}}_{\mathrm{heat},i} \overline{EEV}_i^*(j) + \beta_{T_{\mathrm{oa}}} T^*_{\mathrm{oa}}(j) \tag{1}$$

where β_{EEV} and $\beta_{T_{\mathrm{OA}}}$ are regression coefficients.

The power prediction model can be integrated into the original MPC formulation. The optimization problem seeks the optimal sequence of scaled EEV positions for the prediction time horizon to minimize energy costs, peak demand costs, and comfort violation costs. Given that the power consumption of the OU can be expressed as a linear function of the scaled EEV positions and outdoor air temperatures, it can be formulated as a mixed integer linear problem with temperature and peak demand constraints by slightly reformulating the original MPC formulation as shown in Eq. (2).

$$\begin{aligned}
\min_{\substack{\overline{EEV}_i^*(j)\in\mathbb{R}^+ \\ \delta,\Gamma_{\mathrm{l}},\Gamma_{\mathrm{u}}\in\mathbb{R}^+}} \; & \sum_{j=1}^{N_p}\sum_{i=1}^{n} ER(k+j-1)\left[\beta_{\mathrm{EEV}}\dot{Q}^{\mathrm{r}}_{\mathrm{heat},i}\overline{EEV}_i^*(k+j-1) + \beta_{T_{\mathrm{oa}}}T^*_{\mathrm{oa}}(k+j-1)\right] \\
& + \omega_{\mathrm{d}}\delta + \omega_{\mathrm{l}}\Gamma_{\mathrm{l}} + \omega_{\mathrm{u}}\Gamma_{\mathrm{u}} \\
s.t. \quad & T_{\mathrm{l},i}(k+j) - \Gamma_{\mathrm{l}} \le \hat{\bar{y}}_i(k+j)|k \le T_{\mathrm{u},i}(k+j) + \Gamma_{\mathrm{u}} \;\; (\forall i \in \{1,\dots,n\}) \\
& \beta_{\mathrm{EEV}} \sum_{i}^{n} \dot{Q}^{\mathrm{r}}_{\mathrm{heat},i}\overline{EEV}_i^*(k+j-1) + \beta_{T_{\mathrm{oa}}}T^*_{\mathrm{oa}}(k+j-1) \le \delta \\
& 0 \le \overline{EEV}_i^*(k+j-1) \le 1 \;\; \left(\forall j \in \{1,\dots,N_p\}\right)
\end{aligned} \tag{2}$$

where j is the control timestep from the current timestep k, ER is electricity cost rate [$/kWh], Δt is control timestep (sampling time) of MPC in hour, $\overline{EEV}_i^*$ is the for the is moving-averaged scaled EEV position of ith zone for the sampling time at the $(k+j)$ timestep of the MPC and is the optimization variable}, $\bar{y}_i(k)$ is thermostat temperature measurement at the (k) timestep, $\hat{\bar{y}}_i(k+j)|k$ is the j-step temperature prediction via the building model given the historic data $\left(k = \{\bar{y}_i(k-1), \bar{y}_i(k-2), \dots, \overline{EEV}_i^*(k-1), \overline{EEV}_i^*(k-2), \dots\}\right)$, $\left(T_{\mathrm{l},i}(k+j), T_{\mathrm{u},i}(k+j)\right)$ are the desired heating and cooling setpoints for ith IU, $\omega_{\mathrm{l}}, \omega_{\mathrm{u}}$ $(\in R^+)$ and $\omega_{\mathrm{d}} (\in R^+)$ are weights on variables of

$\Gamma_{\mathrm{l}}, \Gamma_{\mathrm{u}} (\in R^{+})$ and $\delta(\in R^{+})$, δ is an optimization variable for peak demand, Γ_{l} and Γ_{u} are optimization variables for comfort violation.

4. EXPERIMENT

4.1 Experiment Overview

The MPC solution was implemented at the experimental site for a heating week, and its performance is compared with a baseline control. The VRF system is operated with a BACnet interface, and a small computer was installed in the BACnet network as a middleware to collect data and write setpoints. This middleware communicates with the main server computer, which runs the MPC software. After setting up the middleware, we collected 3 weekends of data with setpoint perturbations for system identification. The identified models were then utilized for the MPC solution. Due to space constraints, we have omitted the details of the software architecture for data collection and control interfaces, as well as model training (i.e., system identification) in this paper. However, the procedures and specifics closely mirror those detailed in our previous work (Ham et al., 2024).

4.2 Baseline Control

The Baseline control is typical weekly setpoint schedule that was set up by the building manager. All zones, except for the two private office areas, are conditioned from 7:30 to 18:00, denoting occupied hours. The two aforementioned zones are conditioned from 6:30 to 18:00. During occupied hours, heating and cooling setpoints are maintained at 70ºF (21.1ºC) and 76ºF (24.4 ºC), respectively. The two zones typically unoccupied have heating and cooling setpoints of 68ºF (20ºC) and 76ºF (24.4ºC), respectively. Each zone is equipped with a thermostat providing individual control for ON/OFF functionality and heating and cooling setpoints. Essentially, the Baseline control sets default setpoint schedules, yet occupants can adjust settings as needed. The Baseline control was implemented over a week (April 01-05).

4.3 MPC Settings and Price Signal

The MPC was implemented for a week (Mar 25-29). The comfort boundaries of the MPC are established based on the heating and cooling setpoints of the Baseline control. The MPC updates setpoints every 30 minutes, and this sampling time is determined based on the typical time for achieving setpoints as discussed in Section 3.1. Similar to the Baseline control, occupants have the option to override thermostats. Upon detection of overrides, the MPC ceases to update setpoints for the overridden thermostats. Hourly retail electricity prices (price signal) have been established following a model akin to the CalFUSE tariff, as developed by LBNL (Gerke et al., 2022). The resulting Highly Dynamic Price (HDP) signals exhibit significant price fluctuations throughout the day. The price signal is depicted in Figure 5.

5. RESULTS AND DISCUSSION

5.1 Load Shifting and Peak Demand Reduction

Figure 5 presents a comparison of the average daily VRF power consumption (top) and outdoor air temperature profiles (bottom) between Baseline and MPC days. Each profile for the day is depicted with dimmed lines. The day exhibiting the highest peak demand during the experimental period is marked with a dotted line, and the corresponding peak demand value is annotated with a horizontal dotted line. Peak pricing periods occur from 6-8 and 18-22; however, as the building is vacant after 6 PM, comparisons are drawn only for the morning peak period. Occupancy typically begins at 7:30 AM; during this time, Baseline control shows a significant peak in power and load. In contrast, MPC control initiates heating earlier, resulting in a reduced load at peak times. The power profiles display a zig-zag pattern, primarily due to sudden increases in power when the VRF system activates (start-up). Despite this, the overlap between occupied time and peak pricing is a mere 30 minutes, leading to smoother load profiles and a 24% reduction in load during this interval. Consequently, peak demand decreased by 30%, from 17.2 kW to 11.7 kW. Daily cost savings with MPC are modest at 3%, attributed to the absence of a demand charge in the price signal and minimal overlap time between morning peak price hours and occupied times. It is important to note that the outdoor air temperatures for Baseline and MPC controls were comparable, ensuring a fair comparison for the two cases.

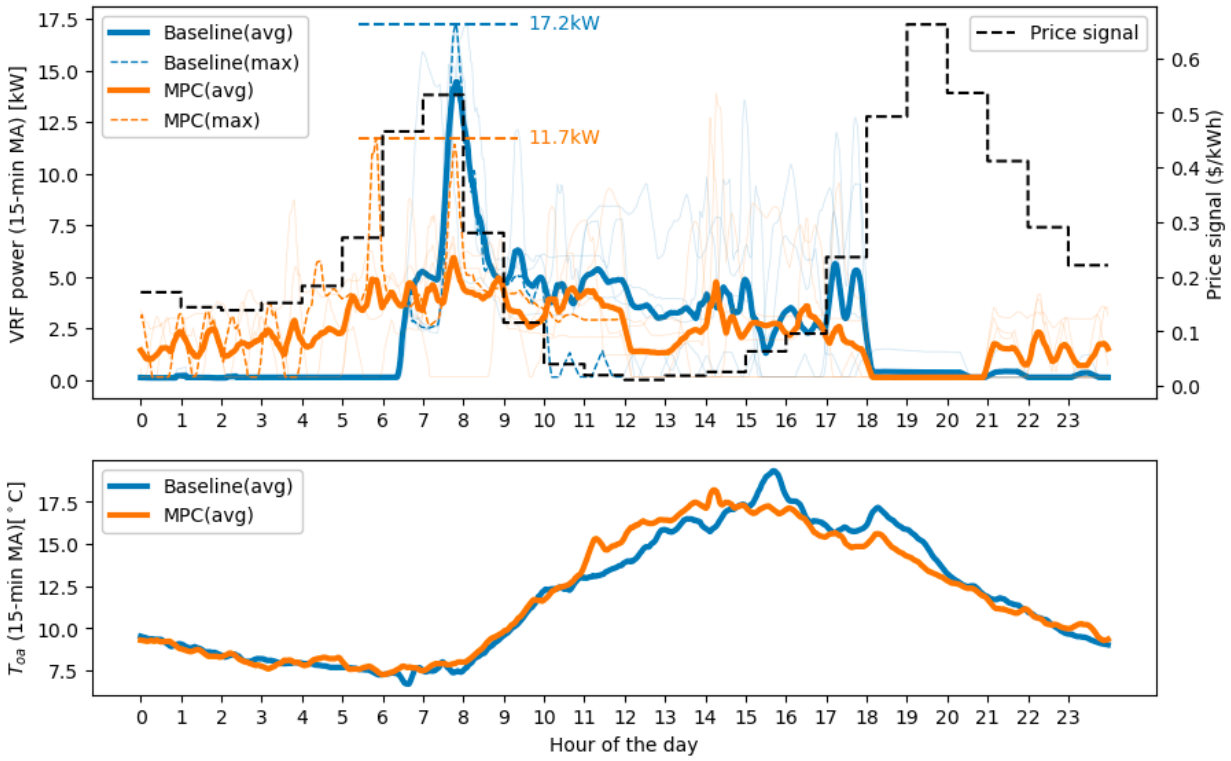

Figure 5. Comparisons of average daily profiles of VRF power (Top) and average daily profiles of outdoor air (Bottom) between Baseline and MPC days; the dimmed profiles indicate daily profiles; the two dotted lines show the maximum peak demand of Baseline and MPC during the trial periods; all data is 15-min moving-averaged which is typical peak demand billing window.

5.2 Discussion and Future Work

The MPC solution performed as expected in the test. However, we identified multiple areas for improvement and further research. Figure 5 illustrates that the load profiles exhibit frequent, significant spikes in power usage. The VRF unit's start-up sequence, in contrast to the simple ON/OFF unit, often leads to unnecessary energy use. By pre-scheduling each FCU's activation with the MPC, we managed to mitigate these spikes by employing 'fan-only' mode in zones without active conditioning. Despite this, not all atypical power usage was eliminated, especially noticeable during daytime hours. For example, zones facing south required cooling demands during the day, unlike other areas. In this case, manual thermostat adjustments by users caused sudden and unpredictable cooling cycles and energy spikes, which we couldn't control. This could be alleviated when we implement the multi-mode VRF MPC that integrates heating, cooling, and simultaneous operation modes into the optimization process. We plan to employ generalized disjunctive programming for this purpose, as outlined in our upcoming research (Kim et al. 2022c).

6. CONCLUSIONS

In this research, we developed a practical MPC solution tailored for SMCBs. The solution was implemented in a lab office building to shift energy usage (load) and reduce costs during peak pricing periods, without the need for additional sensors. We analyzed data to correlate the energy consumption of the VRF system with the control variable (i.e., EEV positions). This correlation (i.e., performance map) was then integrated into our existing MPC solution. We conducted a trial over a heating week in an operational building, comparing the MPC's performance against the Baseline control. The findings revealed a significant 32% drop in peak energy demand and a 3% reduction in energy costs. This was achieved by redistributing 24% of the energy load to non-peak hours, while still giving occupants the freedom to adjust thermostats as needed. Beyond contributing to the understanding of VRF system management, this study provides a practical approach for SMCBs to engage in carbon reduction through GEBs, without sacrificing financial feasibility.

REFERENCES

ASHRAE. (2020). *2020 ASHRAE Handbook: HVAC Systems and Equipment, Chapter 18 SI: Variable Refrigerant Flow*. Atlanta: American Society of Heating, Refrigerating and Air-Conditioning Engineers, Inc.

ASHRAE. (2021). *ASHRAE Guideline 14–2021, High Performance Sequences of Operation for HVAC Systems*. Atlanta: American Society of Heating, Refrigerating and Air-Conditioning Engineers, Inc.

Blum, D., Wang, Z., Weyandt, C., Kim, D., Wetter, M., Hong, T., & Piette, M. A. (2022). Field demonstration and implementation analysis of model predictive control in an office HVAC system. *Applied Energy*, *318*, 119104. https://doi.org/10.1016/j.apenergy.2022.119104

De Coninck, R., & Helsen, L. (2016). Practical implementation and evaluation of model predictive control for an office building in Brussels. *Energy and Buildings*, *111*, 290–298. https://doi.org/10.1016/j.enbuild.2015.11.014

Gerke, B. F., Stuebs, M., Murthy, S., Khandekar, A., Cappers, P., Brown, R. E., & Piette, M. A. (2022). Potential bill impacts of dynamic electricity pricing on California utility customers. *UC Berkeley: California Institute for Energy and Environment (CIEE)*. https://escholarship.org/uc/item/6fr1v1z9

Ham, S. W., Kim, D., Barham, T., & Ramseyer, K. (2023). The first field application of a low-cost MPC for grid-interactive K-12 schools: Lessons-learned and savings assessment. *Energy and Buildings*, *296*, 113351. https://doi.org/10.1016/j.enbuild.2023.113351

Ham, S. W., Paul, L., Kim, D., Pritoni, M., Brown, R., & Feng, J. (2024). Decarbonization of heat pump dual fuel systems using a practical model predictive control: Field demonstration in a small commercial building. *Applied Energy*, *361*, 122935. https://doi.org/10.1016/j.apenergy.2024.122935

Kim, D., Braun, J. E., Cai, J., & Fugate, D. L. (2015). Development and experimental demonstration of a plug-and-play multiple RTU coordination control algorithm for small/medium commercial buildings. *Energy and Buildings*, *107*, 279–293. https://doi.org/10.1016/j.enbuild.2015.08.025

Kim, D., & Braun, J. E. (2018). Development, implementation and performance of a model predictive controller for packaged air conditioners in small and medium-sized commercial building applications. *Energy and Buildings*, *178*, 49–60. https://doi.org/10.1016/j.enbuild.2018.08.019

Kim, D., Wang, Z., Brugger, J., Blum, D., Wetter, M., Hong, T., & Piette, M. A. (2022a). Site demonstration and performance evaluation of MPC for a large chiller plant with TES for renewable energy integration and grid decarbonization. *Applied Energy*, *321*, 119343. https://doi.org/10.1016/j.apenergy.2022.119343

Kim, D., & Braun, J. E. (2022b). MPC solution for optimal load shifting for buildings with ON/OFF staged packaged units: Experimental demonstration, and lessons learned. *Energy and Buildings*, *266*, 112118. https://doi.org/10.1016/j.enbuild.2022.112118

Kim, D., Hong, T., & Piette, M. A. (2022c). Generalized Disjunctive Programming-based, Mixed Integer Linear MPC Formulation for Optimal Operation of a District Energy System for PV Self-consumption and Grid Decarbonization: Field Implementation. *International High Performance Buildings Conference*, *Paper 396*. https://docs.lib.purdue.edu/ihpbc/396/

Langevin, J., Satre-Meloy, A., Satchwell, A. J., Hledik, R., Olszewski, J., Peters, K., & Chandra-Putra, H. (2023). Demand-side solutions in the US building sector could achieve deep emissions reductions and avoid over $100 billion in power sector costs. *One Earth*, *6*(8), 1005–1031. https://doi.org/10.1016/j.oneear.2023.07.008

Li, P., Vrabie, D., Li, D., Bengea, S. C., Mijanovic, S., & O'Neill, Z. D. (2015). Simulation and experimental demonstration of model predictive control in a building HVAC system. *Science and Technology for the Built Environment*, *21*(6), 721–732. https://doi.org/10.1080/23744731.2015.1061888

Neukomm, M., Nubbe, V., & Fares, R. (2019). *Grid-interactive efficient buildings technical report series: Overview of research challenges and gaps*. Office of Energy Efficiency & Renewable Energy, U.S. Department of Energy. https://doi.org/10.2172/1577966

Satchwell, A., Piette, M., Khandekar, A., Granderson, J., Frick, N., Hledik, R., Faruqui, A., Lam, L., Ross, S., Cohen, J., Wang, K., Urigwe, D., Delurey, D., Neukomm, M., & Nemtzow, D. (2021). *A National Roadmap for Grid-Interactive Efficient Buildings*. Lawrence Berkeley National Lab.(LBNL), Berkeley, CA (United States). https://www.osti.gov/servlets/purl/1784302/

Touzani, S., Prakash, A. K., Wang, Z., Agarwal, S., Pritoni, M., Kiran, M., Brown, R., & Granderson, J. (2021). Controlling distributed energy resources via deep reinforcement learning for load flexibility and energy efficiency. *Applied Energy*, *304*, 117733. https://doi.org/10.1016/j.apenergy.2021.117733

U.S. Energy Information Administration (EIA). (2018). *Commercial Buildings Energy Consumption Survey (CBECS) Data*. U.S. Department of Energy.

ACKNOWLEDGEMENT

This work was supported by the Assistant Secretary for Energy Efficiency and Renewable Energy, Building Technologies Office, of the U.S. Department of Energy under Contract No. DE-AC02-05CH11231, by California Energy Commission through grant EPC-19-013, and by CRADA project entitled “Get K-12 Ready for Future Utility Tariff Changes and Aggressive Carbon Reduction Requirements: Wholistic Control Package”.